# Drop impact and wettability: From hydrophilic to superhydrophobic surfaces

Cite as: Phys. Fluids **24**, 102104 (2012); https://doi.org/10.1063/1.4757122
Submitted: 29 June 2012 . Accepted: 10 September 2012 . Published Online: 16 October 2012

Carlo Antonini, Alidad Amirfazli, and Marco Marengo

# Drop impact and wettability: From hydrophilic to superhydrophobic surfaces

Carlo Antonini,[1] Alidad Amirfazli,[2] and Marco Marengo[1,a)]
[1]*Department of Industrial Engineering, Università degli Studi di Bergamo, Viale Marconi 5, 24044 Dalmine (BG), Italy*
[2]*Department of Mechanical Engineering, University of Alberta, Edmonton, Alberta T6G 2G8, Canada*

(Received 29 June 2012; accepted 10 September 2012; published online 16 October 2012)

Experiments to understand the effect of surface wettability on impact characteristics of water drops onto solid dry surfaces were conducted. Various surfaces were used to cover a wide range of contact angles (advancing contact angle from 48° to 166°, and contact angle hysteresis from 5° to 56°). Several different impact conditions were analyzed (12 impact velocities on 9 different surfaces, among which 2 were superhydrophobic). Results from impact tests with millimetric drops show that two different regimes can be identified: a moderate Weber number regime ($30 < We < 200$), in which wettability affects both drop maximum spreading and spreading characteristic time; and a high Weber number regime ($We > 200$), in which wettability effect is secondary, because capillary forces are overcome by inertial effects. In particular, results show the role of advancing contact angle and contact angle hysteresis as fundamental wetting parameters to allow understanding of different phases of drop spreading and beginning of recoiling. It is also shown that drop spreading on hydrophilic and superhydrophobic surfaces occurs with different time scales. Finally, if the surface is superhydrophobic, eventual impalement, i.e., transition from Cassie to Wenzel wetting state, which might occur in the vicinity of the drop impact area, does not influence drop maximum spreading. © *2012 American Institute of Physics*. [http://dx.doi.org/10.1063/1.4757122]

## I. INTRODUCTION

In the last decade industry has shown an increasing interest in the potential application of superhydrophobic surfaces (SHSs), i.e., water repellent surfaces. Superhydrophobicity facilitates water shedding from surfaces and decrease surface contamination, to give the so-called self-cleaning effect. The application of SHS would be in many fields, such as water management in fuel cells[1] and in icing mitigation.[2]

To characterize the surface wettability and to investigate the physics of drop-surface interaction, two approaches are commonly used: a static (or quasi-static) approach, using sessile drops, and a dynamic approach, by means of drop impact studies. With respect to drop impact studies, a wide number of works in literature is dedicated to the investigation of single and multiple drop impact on solid surfaces (see reviews[3,4]). Majority of studies, either experimental,[5–7] numerical,[8,9] or theoretical,[10,11] mainly refer to surfaces with high wettability (i.e., hydrophilic, when liquid is water), for which the contact angle (CA or $\theta$), i.e., the angle formed at the three phase line, is lower than 90°. Only a small number of studies investigated surfaces with contact angles higher than 120°.[12–17]

The influence of wettability was first highlighted by Hartley and Brunskill,[18] who showed the role of wettability in achieving drop rebound after impact onto leaves. The authors proposed an energy

a)Author to whom correspondence should be addressed. Electronic mail: marco.marengo@unibg.it.

 

balance approach for the spreading lamella, in which they accounted for wettability through the value of a static contact angle. A phenomenological approach to drop impact on SHS was recently given by Rioboo *et al.*,[17] where four different outcomes were identified: deposition, rebound, sticking, and fragmentation. Accordingly, a drop impact regime map was proposed. It was observed that, for the specific system analyzed (water drops on superhydrophobic polypropylene surface), the transition from rebound to fragmentation was governed by Weber number, $We = \rho V^2 D_0/\sigma$ ($\rho$ is density, $V$ is the impact speed, $D_0$ is the drop initial diameter, and $\sigma$ is the surface tension); threshold $We$ value between two regimes was near 60. For the deposition-rebound limit, it was experimentally observed that the transition does not only depend on the $We$ number. It was proposed in Ref. 17 that the transition depends on $We$ and on two solid surface parameters: the average contact angle, defined as the average between advancing, $\theta_A$, and receding, $\theta_R$, contact angles, and the contact angle hysteresis, $\Delta\theta$ (contact angle definitions are discussed in Sec. II).

Drop rebound time[19] (i.e., time between impact and rebound instants, also referred to in literature as residence time[20] or contact time[16]) on SHS was studied by Quéré and co-workers.[13,14,16] It was found that, in the investigated $We$ range ($0.3 < We < 37$ in Ref. 16), drop rebound time on a SHS does not depend on impact speed, $V$, but only scales with drop mass, $m$, and liquid surface tension, $\sigma$:

$$t_{\text{rebound}} = 2.6\left(\frac{\rho D_0^3}{8\sigma}\right)^{1/2}. \tag{1}$$

The formula reveals that there are strong analogies between drop impacting on a SHS and on a hot surface in Leidenfrost conditions (i.e., when a vapor film forms at the liquid-solid interface due to drop fast evaporation, because the surface temperature exceeds Leidenfrost temperature). In 1966, Watchers and Westerling[20] measured that the rebound time of a drop impacting on a surface in Leidenfrost conditions was close to the first-order vibration period of a freely oscillating drop,[21] equal to $\pi/\sqrt{2}\left(\rho D_0^3/8\sigma\right)^{1/2}$, which is the so-called Rayleigh time (or drop free oscillation time). Note that the only difference between the rebound time in Eq. (1), valid for SHS, and the Rayleigh time is the numerical pre-factor, being rebound time 17% longer than Rayleigh time. A similar difference was also measured by Chandra and Avedisian,[19] who measured that for a 1.5 mm drop impacting on a hot surface in Leidenfrost conditions, drop rebound time is ~30% higher than the Rayleigh time.

Bartolo *et al.*[12] focused on the retraction dynamics of water drops on Parafilm®, which has a receding contact angle equal to 80° (as such, coating is weakly hydrophobic). They identified two different regimes (capillary-inertial and capillary-viscous) for drop retraction dynamics. For the specific tested surface, threshold between two regimes was found to be $Oh = 0.02$ ($Oh = \mu/\sqrt{\rho\sigma D_0}$ is the Ohnesorge number, where $\mu$ is water viscosity). Li *et al.*[22] investigated the effect of surface texturing on the receding phase and thus drop contact time. Tests performed on textured silicon surfaces decorated by square arrays of pillars with different geometries showed that surface texture has a direct effect on receding contact angle and thus modifies retraction dynamics and, in case of rebound, drop rebound time.

Although many papers have been devoted to understanding drop impact on dry surfaces, we found some inconsistencies in literature. As explained in our recent review,[4] and also as briefly discussed in Sec. III of the present paper, correlations in literature disagree on different issues, e.g., the relation between drop maximum spreading and impact speed, and whether or not surface wettability influences the different phases of drop impact. As such, we decided to investigate drop impact on nine surfaces using a wide range of surface wettabilities, trying to understand the combined effect of different parameters, such as impact conditions (in particular, $We$) and surface properties, e.g., advancing and receding contact angles, $\theta_A$ and $\theta_R$, respectively.

## II. HOW TO CHARACTERIZE SURFACE WETTABILITY

A key issue to understand the effect of surface wettability during drop impact on a surface is how to characterize wettability, i.e., which parameters should be used as a quantitative measure.

Most of the works in literature rely on the evaluation of the equilibrium contact angle, $\theta_{eq}$ (see, e.g., Refs. 23–25). However, the measurement of an equilibrium contact angle on a real surface is questionable, since metastable configurations for a sessile drop on a surface are possible and different values of the contact angle can be measured.[26] For this reason, at least two contact angle values should be measured and reported as a measure of wettability: the advancing, $\theta_A$, and the receding, $\theta_R$, contact angles, which are measured on a horizontal surface while quasi-statically expanding and contracting a drop, respectively. The difference between the two values is referred to as contact angle hysteresis (CAH or $\Delta\theta$), and is often used as a reference parameter to measure drop mobility on a surface: the lower the contact angle hysteresis, the higher the mobility and the easier the drop removal.[27] Other measurements of the contact angle can be given, e.g., maximum and minimum contact angle, $\theta_{\max}$ and $\theta_{\min}$, respectively, which are measured for a drop on a tilted surface[28] or for a drop exposed to aerodynamic surfaces[29] at the moment of incipient motion. A surface can be defined superhydrophobic when both advancing and receding contact angles are high (an arbitrary threshold, usually found in the literature, is 150°) and contact angle hysteresis is small (lower than 10°).

As a further consideration, drop impact is not a quasi-static process and different dynamic contact angles can be observed, depending on the impact conditions and contact line velocity. Numerical simulations, which require values of contact angles to be specified as a boundary condition, often rely on specific laws (e.g., Refs. 30 and 31), which provide the value of the dynamic contact angle as a function of the equilibrium contact angle and the capillary number, $Ca = \mu V_{cl}/\sigma$, defined using the contact line velocity, $V_{cl}$. Use of such laws to apply the correct boundary conditions at three phase line is still widely used, as demonstrated in a recent study by Roisman *et al.*,[32] who used the correlation by Kistler[31] and demonstrated good agreement between numerical simulations and experiments for low *We* numbers ($0.9 < We < 8$) for one specific case with $\theta_{eq} = 120°$. However, the application of usual boundary conditions, such as laws predicting the dynamic contact angle and the no-slip condition at the liquid-surface interface, does not necessarily apply to the case of drop impact on SHS.[33,34] Different methodologies to measure contact angles point out that the choice of one or more parameters to synthetically define wettability is not a trivial issue, and care must be taken in correlating contact angles measured in quasi-static conditions to study strongly dynamic phenomena.[29]

## III. CORRELATIONS AND MODELS FOR DROP SPREADING

One of the most important parameters used to describe drop impact on a surface is the drop maximum spreading, expressed by the maximum spread factor, $\xi_{\max} = D_{\max}/D_0$ (ratio between the contact diameter at maximum spreading, $D_{\max}$, and drop diameter before impact, $D_0$). Many correlations and models have been proposed in literature,[5,11,14,15,24] as well as 1D analytical models,[25,35,36] which predict time evolution of spread factor $\xi(t) = D(t)/D_0$.

Two correlations for $\xi_{\max}$[5,11] were formulated investigating drop impacts on hydrophilic surfaces, using water as liquid, and glass or metal as impact surfaces. The correlation proposed by Scheller and Bousfield[5] is

$$\xi_{\max} = 0.61\,(We/Oh)^{0.166} \tag{2}$$

and a more recent semi-empirical correlation by Roisman,[11] based on a combination of theoretical results and experimental data fitting, is

$$\xi_{\max} = 0.87Re^{1/5} - 0.40Re^{2/5}We^{-1/2}, \tag{3}$$

where $Re = \rho V D_0/\mu$ is the Reynolds number. Clanet *et al.*[14] performed test on a SHS, with a static contact angle of 170° (details on contact angle hysteresis and composition of the surface were not provided). It was claimed that the experimental data on maximum spreading are well fit by the correlation:

$$\xi_{\max} = 0.9\,We^{1/4} \tag{4}$$

for Weber numbers in the range $3 < We < 300$ (see Figure 2 in Ref. 14). In the same study,[14] the authors also claimed that Eq. (4) represents also well their experimental data for water impacting on a hydrophilic plastic surface, and experimental data obtained by Stow and Hadfield[37] for water impacting a smooth aluminum plate, and by Marmanis and Thoroddsen[38] for water impacting a thick linen paper, with Weber numbers in the range $3 < We < 3000$ (see Figure 8 in Ref. 14). As such, the authors claim the surface wettability does not play a role in maximum spreading of drop, not even for low $We$.

Two other studies in literature[15,24] proposed a correlation for $\xi_{\max}$, based on an energy balance approach between the moment of impact and the moment of maximum spreading. In both studies, effect of surface wettability is taken into account. In Pasandideh-Fard *et al.*,[24] an explicit equation for $\xi_{\max}$ was given:

$$\xi_{\max} = \sqrt{\frac{We + 12}{3\,(1 - \cos\theta) + 4\left(\frac{We}{\sqrt{Re}}\right)}}. \tag{5}$$

According to Mao *et al.*,[15] maximum spreading can be found as the real root of the following cubic equation:

$$\left[\frac{1}{4}\,(1 - \cos\theta) + 0.2\frac{We^{0.83}}{Re^{0.33}}\right]\xi_{\max}^3 - \left(\frac{We}{12} + 1\right)\xi_{\max} + \frac{2}{3} = 0. \tag{6}$$

In the present paper, the value of the advancing contact angle, $\theta_A$, is used instead of the static contact angle, $\theta$, as in the original works.[15,24] As explained in Sec. II, multiple values of the contact angle can be observed, not only a single equilibrium value. As such, advancing contact angle, $\theta_A$, was chosen as characteristic contact angle to describe spreading, since the drop contact line advances during spreading phase.

Many open questions arise from the comparison of the above five correlations. First, all correlations agree that the maximum spread factor, $\xi_{\max}$, increases with velocity following a power law $\xi_{\max} \propto V^{\alpha}$. However, different correlations disagree on the value of the exponent, $\alpha$. In high Weber and Reynolds number regime, i.e., when the effects of wettability are secondary compared to inertial effects, $\alpha$ varies from 0.33,[5] to 0.50.[14] According to models that account for surface wettability, $\alpha$ is a function of contact angle, with $0.23 < \alpha < 0.38$[24] and $0.32 < \alpha < 0.45$,[15] lower and upper limits for $\alpha$ found for contact angles equal to 0° and 180°, respectively. Second, according to Clanet *et al.*,[14] viscosity and surface wettability do not affect the maximum spreading, not even at low to moderate Weber numbers ($We$ in the order of unities or tens): the correlation in Eq. (4)[14] shows that maximum spreading is only a function of $We$. This result differs from all other correlations above, which include viscosity (through either Reynolds number or Ohnesorge number); two correlations seen in Refs. 15 and 24, as well as two 1D models of Refs. 35 and 36 also include the effect of surface wettability through the contact angle. Given the disagreement between different models, experiments were aimed at understanding if, and eventually under which conditions, wettability has an effect on drop spreading on a dry solid surface for a wide range of surface wettabilities.

## IV. METHODS AND MATERIALS

Drop impact tests were performed on the following surfaces: (i) untreated smooth glass; (ii) poly(methyl methacrylate) (PMMA); (iii) Teflon; (iv) SHS-Teflon; (v) OTSa; (vi) OTSb; (vii) OTSc; (viii) OTSd; and (ix) SHS-Zonyl. For surfaces (ii), (iii), (iv), (ix), aluminum served as substrate on which various coatings were applied, whereas smooth microscope glass was used for surfaces (v) to (viii). Surface (ii) was spray coated, depositing a thin layer of PMMA (a solution 1% (w/w) PMMA dissolved in dry toluene was used). Samples (iii) and (iv) were both spray coated, depositing a thin layer of Teflon® over the surface; for sample (iii), Teflon was directly applied onto smooth aluminum sheet; for sample (iv), aluminum substrate was first etched in acid solution, to achieve the desired surface roughness, and then sprayed with Teflon. To etch aluminum, a 36% (v/v) solution of hydrochloric (HCl) acid in deionized water was used. The aluminum sheet was immersed into

TABLE I. Advancing ($\theta_A$) and receding ($\theta_R$) contact angle, contact angle hysteresis ($\Delta\theta$), surface mean roughness, $R_a$, and rms roughness, $R_q$, for all tested surfaces. Standard deviation for contact angles is $\pm 2^\circ$.

| | Surface | $\theta_A$ (°) | $\theta_R$ (°) | $\Delta\theta$ (°) | $R_a$ ($\mu$m) | $R_q$ ($\mu$m) |
|---|---|---|---|---|---|---|
| i | Glass | 48 | <5 | >43 | $0.04 \pm 0.01$ | $0.05 \pm 0.01$ |
| ii | PMMA | 90 | 34 | 56 | $0.50 \pm 0.10$ | $0.75 \pm 0.15$ |
| iii | Teflon | 123 | 98 | 25 | $0.50 \pm 0.15$ | $0.60 \pm 0.20$ |
| iv | SHS-Teflon | 162 | 154 | 8 | $2.7 \pm 0.5$ | $3.4 \pm 0.5$ |
| v | OTSa | 111 | 90 | 21 | $0.04 \pm 0.01$ | $0.04 \pm 0.01$ |
| vi | OTSb | 102 | 85 | 17 | $0.04 \pm 0.01$ | $0.04 \pm 0.01$ |
| vii | OTSc | 60 | <10 | >50 | $0.04 \pm 0.01$ | $0.04 \pm 0.01$ |
| viii | OTSd | 72 | 32 | 40 | $0.04 \pm 0.01$ | $0.04 \pm 0.01$ |
| ix | SHS-Zonyl | 166 | 161 | 5 | $2.4 \pm 0.6$ | $3.0 \pm 0.7$ |

the acid solution for 1.5 min, allowing optimal surface texture to develop. The Teflon coating used for samples (iii) and (iv) was obtained with a 10:1 (v/v) solution of FC-75 and Teflon from DuPont™. Once solution was applied, samples were placed in a vacuum oven (34 mbar) at 120 °C for 1 h. Surfaces (v) to (viii) were grafted with octadecyltrichlorosilane ($C_{18}H_{37}Cl_3Si$), following the procedure described in detail in Ref. 39; each sample was exposed to UV for different times to modify the contact angles (maximum exposure time was 4 min for surface (viii)). Surface (ix) was spray coated using a method described in Ref. 40 (see also Ref. 41); surface (ix) was prepared using Zonyl 8740® from DuPont as fluorinated component and 3M™ Scotch-Weld™ Threadlocker TL62 as adhesive component.

All surfaces were characterized by measuring advancing ($\theta_A$) and receding ($\theta_R$) contact angles using the sessile drop method, and measuring both surface mean roughness, $R_a$, and rms roughness, $R_q$, using a roughness meter (Diavite DH-5, resolution 0.01 $\mu$m). Results from measurement are reported in Table I. Use of nine different surfaces allows to cover a wide range of advancing and receding contact angles ($48^\circ < \theta_A < 166^\circ$; $5^\circ < \theta_A < 161^\circ$) and contact angle hysteresis ($5^\circ < \Delta\theta < 56^\circ$).

For single drop impact tests, typical test apparatus for drop impact studies was used: drop is generated at the tip of a needle, then is accelerated by gravity and impacts normally on a surface. Images of drop impact were recorded using a high-speed camera (PCO 1200-hs) with a frame rate up to 21 000 fps and pixel resolution in the range 12–30 $\mu$m (depending on magnification and required field of view).

Figure 1 illustrates two image sequences for a drop impacting on PMMA and SHS-Teflon ($D_0 = 2.83$ mm, $V = 2$ m/s). Most images were recorded from side (horizontal camera positioning); for those tests, where presence of secondary drops disturbed observation from side (typically on SHS at high $We$ numbers), images were recorded mounting the camera with a tilt angle of 19°. When the drop impact is observed mounting the camera with a tilt angle, the rim can be identified clearly even if significant splash and fingering are present: the spread diameter is taken as the measured diameter of the edge of the rim. Rim measurements were performed manually, since automatic edge detection was not possible. It should be noted that, even at high $We$, the standard deviation of $D_{\max}$ measurement was ~1%.

Images were automatically analyzed using a code, developed in MatLab® environment; the image analysis code provided the following information: (1) time evolution of contact diameter, $D(t)$, and spread factor $\xi(t) = D(t)/D_0$; (2) maximum spread factor, $\xi_{\max} = D_{\max}/D_0$; (3) spreading time, $t_S$; (4) time at maximum spreading, $\Delta t_{\xi_{\max}}$, i.e., the time delay between the moment drop stops spreading and the moment drop starts receding; and (5) drop rebound time, if drop rebounds. Time at maximum spreading, $t_S$, is defined as the time when $D = 0.99 D_{\max}$; time at maximum spreading, $\Delta t_{\xi_{\max}}$, is the time interval in which $D > 0.99 D_{\max}$.

Drop diameter was kept constant ($D_0 = 2.86$ mm $\pm$ 1%), velocity was varied from 0.90 to 4.2 m/s (±0.6%), to give a constant Ohnesorge number ($Oh = 0.002 \pm 0.5\%$), and Weber numbers in the range $30 < We < 685$ (±2.2%).

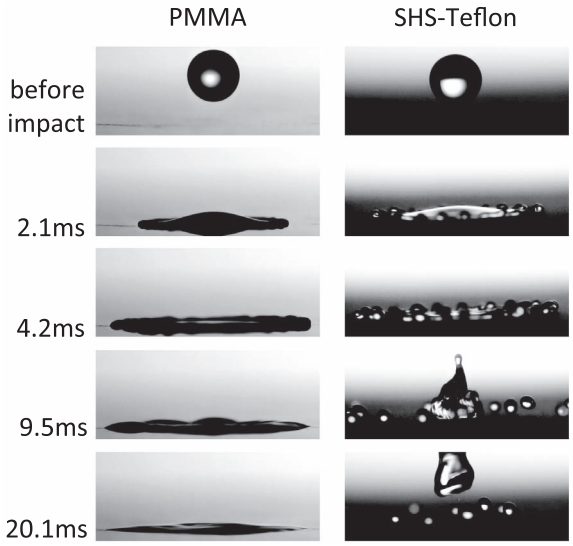


FIG. 1. Image sequence of water drop impacting on a dry surface ($D = 2.83$ mm, $V = 2.0$ m/s, and $We = 150$). Surfaces are PMMA (left column) and SHS-Teflon (right column). Water drop rebound can be observed on SHS-Teflon surface.

## V. RESULTS AND DISCUSSION

### A. Maximum spread factor

Figure 2 illustrates maximum spread factor, $\xi_{max}$, as function of the advancing contact angle, $\theta_A$, for different ranges of $We$. Two regimes can be clearly identified: for moderate $We$ number ($25 < We < 200$), $\theta_A$, i.e., surface wettability has an effect on $\xi_{max}$; for high $We$ number ($We > 200$), $\xi_{max}$ becomes independent from $\theta_A$ and is only a function of $We$.

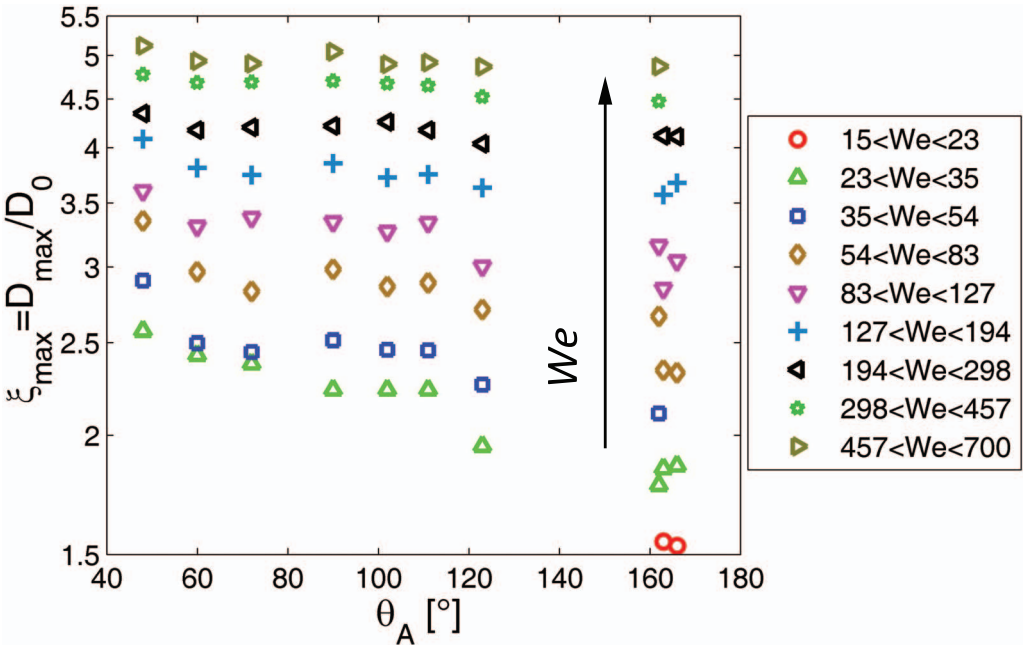


FIG. 2. Drop maximum spreading, $\xi_{max}$, as function of advancing contact angle, $\theta_A$, for different ranges of Weber number, $We$ (see legend). The data points in each $We$ range represent the average of experimental values in the specified range. Error bars for $\xi_{max}$ are not included here because data are averaged over pre-defined $We$ ranges. Experimental uncertainty for a given $We$ number is indicated in Figure 3.

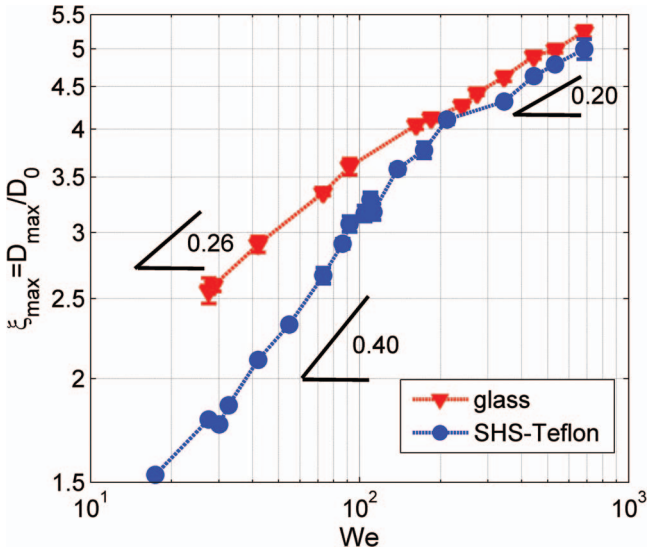


FIG. 3. Drop maximum spreading, $\xi_{max}$, as function of Weber number, $We$, for glass (most hydrophilic surface) and SHS-Teflon. Values of the curve slopes, $b$ (evaluated fitting experimental data with power law in the form $\xi_{max} = aWe^b$, for $We < 200$ and $We > 200$) are indicated on the graph. For high Weber number ($We > 200$), the slope was obtained fitting experimental data from all surfaces. Error bars, denoting one standard deviation, are in most cases smaller than the symbol size. Lines are to guide the eyes.

Figure 3 shows dependence of $\xi_{max}$ on $We$ for the most hydrophilic surface, glass, and one SHS, i.e., SHS-Teflon. Data in Figure 3 highlight the existence of two distinct impact regimes: at $We = 30$, $\xi_{max}$ is 30% lower on SHS-Teflon, compared to glass. For moderate Weber ($We < 200$), maximum spreading is affected by surface wettability. Note that repeatability of data is high: error bars in Figure 3, denoting one standard deviation, are in most cases smaller than the symbol size. Fitting the experimental data in this range with a power law (the common feature of literature correlations), one finds $\xi_{max} \propto We^{0.26} \propto V^{0.52}$ for glass and $\xi_{max} \propto We^{0.40} \propto V^{0.80}$ for SHS-Teflon. At high Weber regime ($We > 200$), the two curves in Figure 3 have the same slope and almost overlap; fitting data from all surfaces gives $\xi_{max} \propto We^{0.20} \propto V^{0.40}$; note that, in the high Weber regime, the experimental value of the velocity exponent, $\alpha = 0.40$, falls within the range seen in literature, i.e., 0.23–0.5.

With respect to impacts on SHS, one may think of violation of no-slip condition to explain different drop spreading, compared to other surfaces. However, most of the models and correlations[5,11,15,24,25,36] agree that an increase of viscous dissipation causes a reduction of maximum contact diameter, since kinetic energy is dissipated instead of being converted into surface energy. The eventual slip at the liquid-solid interface on SHS should cause a reduction of energy dissipation, and thus lead to an increase of maximum contact diameter. However, experimental data clearly show that, for impacts on SHS at moderate $We$, the contact diameter is lower than on all other surfaces. Therefore, the effect of capillary forces dominates the drop impact and it is not possible to appreciate "macroscopically" a possible violation of no-slip condition at liquid-solid interface.

As an additional observation, drop spreading on the two different SHS is similar and no significant differences were measured during the spreading phase for SHS. Noticeably, similar spreading behavior was observed even at higher speeds, despite a different resistance to surface impalement,[42,43] which was observed on the two surfaces: drop remains in a Cassie-Baxter (or "composite") state on SHS-Teflon (as substantiated by full rebound of drop) for all test conditions, whereas on SHS-Zonyl a transition to Wenzel (or "sticky") state occurs in the vicinity of the drop impact point (drops only partially rebound after recoiling and do not roll away as easily as on SHS-Teflon, if surface is tilted after impact)—see Annex A of the supplementary material.[44] As such, it can be concluded that the eventual liquid impalement in the area close to the impact point does not influence maximum spreading of a drop.

The comparison between experimental data and models (see Tables S1 and S2 in Annex B of the supplementary material[44]) shows that none of the models is able to capture the trends highlighted in Figure 3 for both glass and SHS-Teflon. The poor correspondence between models and experiments highlights the limit of energy balance approaches: most of the models[5,15,21,22,32] require an adjustment for the energy dissipation term to best fit the experimental data, because some effects, e.g., edge effects associated with the rim formation are not always properly accounted for.[10,11] For this reason, models are not capable to predict the two impact regimes identified experimentally.

In conclusion, analysis of drop maximum spreading on dry surfaces highlights that effect of wettability can be observed for millimetric drop impacting at $We$ lower than 200. To predict maximum spreading on hydrophilic surfaces, the correlation found in the literature with the lowest error in the investigated range is Roisman correlation. For SHS, no correlation at present is capable to represent different trends for $\xi_{\max}$ at moderate and high $We$ (with the slope of the curve $\xi_{\max}(We)$ changing from 0.40 to 0.20 in a logarithmic plot, see Figure 3).

### B. Drop impact scaling time

Drop impact characteristic times are of particular interest in processes where heat transfer is involved, e.g., drop solidification. In this section the time scaling for drop impact onto the most hydrophilic (glass) and one superhydrophobic surface (SHS-Teflon) is analyzed. In Secs. V C and V D, a comparison between spreading time and time at maximum spreading for all surfaces is also presented.

Figure 4 illustrates the time evolution of the drop diameter, made non-dimensional by the maximum contact diameter, i.e., $D(t)/D_{\max}$, on glass (Figure 4(a)) and SHS-Teflon (see Figure 4(b)). Drop spreading evolution at different $We$ is reported. For glass (see Figure 4(a)), all curves in the investigated range ($30 < We < 685$) collapse onto a single curve if time is normalized with $V^{-0.5}$, suggesting that drop characteristic times likely scales with $We^{-0.25}$. Note that all curves overlap, not only in the spreading, but also at the beginning of the recoil phase. Such result highlights that spreading time is not directly proportional to the convective time, $D_0/V$, which is often used in the literature to make time non-dimensional for drop impact analysis. Differently, on the SHS-Teflon (Figure 4(b)) all curves collapse onto a single curve without normalizing the time, i.e., drop spreading time does not depend on impact speed in the range investigated ($29 < We < 276$). Note that automatic image analysis at $We = 276$ was performed up to 1 ms, when the ejection of a

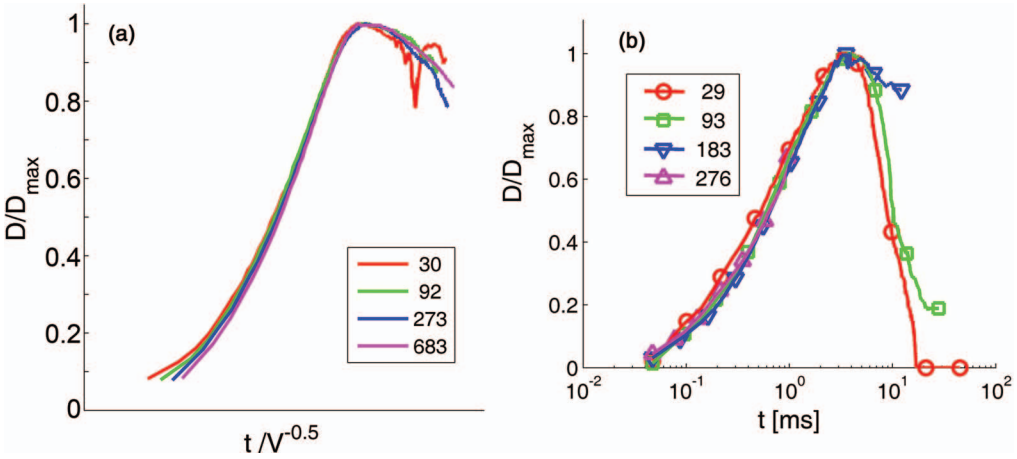


FIG. 4. Time evolution of drop contact diameter scaled by maximum contact diameter, $D(t)/D_{\max}$, on glass (a) and on SHS-Teflon (b) at different Weber numbers, $We$ (indicated in the legend). (a) Time is normalized by $V^{-0.5}$ (values on x axis are not indicated because quantity $t/V^{-0.5}$ has no physical meaning); (b) time is in ms. Note that automatic image analysis at $We = 276$ was performed up to 1 ms, when the ejection of a secondary drop from the rim occurs and does not allow an automatic measure of the contact diameter; for $We = 276$, $D_{\max}$ was determined manually, in order to calculate $D(t)/D_{\max}$. Lines are to guide the eyes.

secondary drop from the rim occurs and does not allow an automatic measure of the contact diameter. Curves at $We$ up to 183 overlap quite well even in the recoil phase, although automatic image analysis was complicated during this phase by receding break-up (see Rioboo *et al.*[45]). Nevertheless, manual image analysis confirmed that drop evolution during receding phase is similar, as also confirmed by the fact that drop rebound time is constant and independent from drop impact velocity (as already shown in Ref. 16). The different time scaling highlights that dynamic interaction between water and a SHS is qualitatively different from the interaction between water and a hydrophilic surface.

On a SHS, drop behaves almost as an ideal mass-spring system: as shown by Richard *et al.*,[16] drop rebound time is associated to the oscillation time, which is proportional to the square root of the ratio between mass, $m$, and surface tension, $\alpha$. Thus, drop dynamic times are determined only by drop physical properties and do not depend on impact speed, at least in the moderate $We$ regime, when a liquid like water is used. On hydrophilic surface, the trend is different. For a drop impacting on a hydrophilic surface, results show that drop spreading deviates from the elastic response, which is typical of SHS (as observed on SHS-Teflon). The difference can likely be attributed to the combined effect of capillary forces (which tends to enhance the spreading) and the strong damping mainly associated to viscous dissipation in the lamella boundary layer: as on a oscillating mass-spring system the oscillation time is modified by a damper, damping due to viscous dissipation on a hydrophilic surface increases the oscillation time (or equivalently, decreases frequency). Analytical models, such as model by Attané *et al.*,[36] show that a drop impacting on a surface can be modeled by a second order model ODE, as a mass-spring system with damping, the only difference being the presence of nonlinear terms for ODE (Ordinary Differential Equation) modeling drop impact. We can thus conclude that, for a drop impacting on a hydrophilic surface, drop characteristic times are affected by impact speed, since boundary layer shape and velocities strongly depend on impact conditions, in particular, $Re$ (see Roisman *et al.*[10]).

### C. Spreading time

Drop spreading time, $t_S$, as function of $We$ is illustrated in Figure 5. For moderate Weber numbers, surface wettability influences spreading time: at $We = 30$, spreading time varies from a minimum of 3.1 ms on SHS-Teflon to a maximum of 4.7 ms on glass. On one hand, it can be observed that on most hydrophilic surfaces, like glass, spreading time appears proportional to $We^{-0.25}$, as already discussed in Sec. V B, and the trend is similar at both moderate and high $We$. On the other hand, at moderate $We$, for OTSa and OTSb the spreading time slightly decreases for increasing $We$, whereas both on the smooth hydrophobic surface with the highest advancing contact angle (Teflon, $\theta_A = 123^\circ$) and on the superhydrophobic surface (SHS-Teflon, $\theta_A = 165^\circ$), spreading time remains constant (considering the experimental uncertainty). For high Weber numbers ($We > 200$), where inertia dominates capillary effects, spreading time mainly depends on impact $We$ number and effect of wettability is secondary: all curves from different surfaces converge to a line at high $We$, with a slope $We^{-0.25}$ on a logarithmic scale (see Figure 5). The only curve that is somewhat separated from others is the SHS-Teflon curve. Note, however, that difference between SHS-Teflon and other surfaces is related to drop break-up, at the end of spreading phase, which occurs only for SHS-Teflon at high Weber numbers, i.e., the rim breaks up in small secondary drops, which are ejected outwards and do not recoil towards the impact point as for all the other surfaces. The occurrence of drop break-up on SHS-Teflon can be seen in Figure 1: the sequence (impact at $We = 150$) shows drop break-ups after maximum spreading has been reached. For higher impact energy, the intensity of drop break-up increases and occurs in the final phase of spreading (when rim decelerates and contact line speed approaches zero). To clearly highlight the occurrence of drop break-up, a dotted line is used in Figure 5 for SHS-Teflon data at high impact speed.

To sum up findings on spreading characteristic time, millimetric water drop impacts behave differently at moderate and high $We$ numbers: at moderate $We$ (<200), spreading time does not depend on impact energy on SHS, whereas on hydrophilic surfaces time is proportional to $V^{-0.50}$; at high $We$ (>200), the effects of wettability become secondary and spreading time becomes proportional to $V^{-0.50}$ for all surfaces.

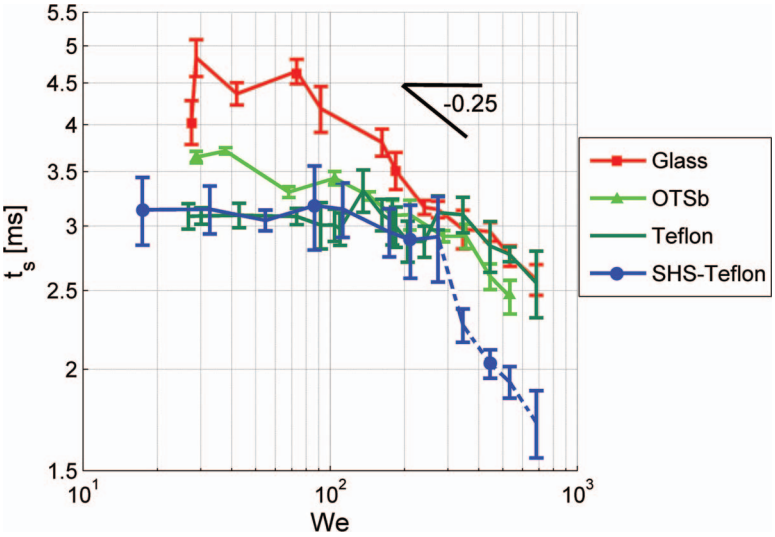


FIG. 5. Experimental data for spreading time, $t_S$, as function of Weber number, $We$. Error bars denote one standard deviation. Lines are to guide the eyes. The line corresponding to the highest Weber numbers for SHS-Teflon is dotted, to highlight the drop break-up in the final stages of spreading (see text for more details).

### D. Time at maximum spreading

Drop impact dynamics is usually classified in the literature in three different phases, i.e., spreading, recoil, and drop oscillation (or eventually rebound). However, the analysis of contact diameter evolutions shows the time, while drop is at maximum spreading, $\Delta t_{\xi_{max}}$ (in other words, the time shift between the moment the drop stops spreading and when it starts recoil), is in the order of few milliseconds (up to 8 ms—see Figure 6), and can be even higher than the spreading time, $t_S$. This means that an intermediate phase needs to be introduced in analysis of drop impacts.

Figure 6 illustrates the value of $\Delta t_{\xi_{max}}$ as function of $We$, for four different surfaces (glass, OTSb, Teflon, and SHS-Teflon). The trend $\Delta t_{\xi_{max}}$ is to some extent similar to the trend of the spreading

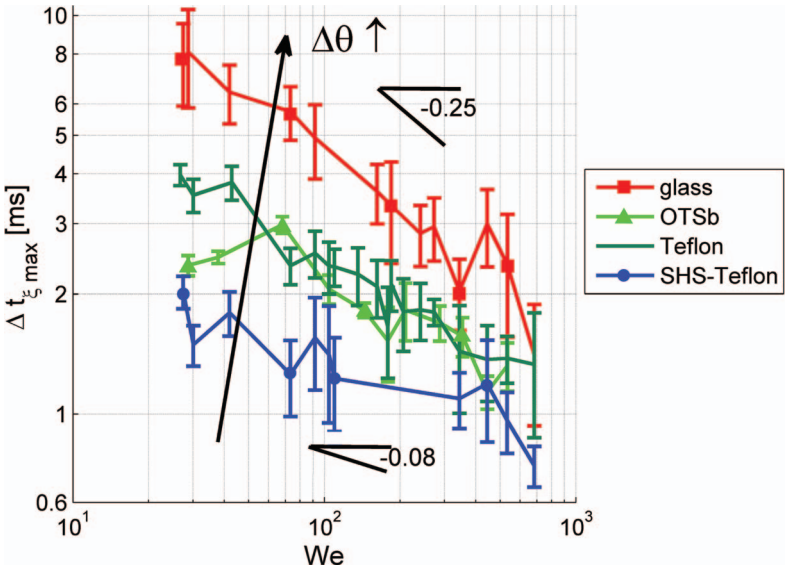


FIG. 6. Experimental data for time at maximum spreading, $\Delta t_{\xi max}$ (see definition in Sec. IV) as function of Weber number, $We$. Lines are to guide the eyes. Error bars denote one standard deviation.

time, $t_S$ (see Figure 5): $\Delta t_{\xi_{\max}}$, which decreases with increasing $We$ and with decreasing wettability. However, main differences can be observed: first, the most important wetting parameter to affect $\Delta t_{\xi_{\max}}$ is the contact angle hysteresis, $\Delta\theta$, rather than the advancing contact angle, $\theta_A$, as for $t_S$; and second, a distinction between moderate and high $We$ numbers is not as apparent for $\Delta t_{\xi_{\max}}$ as it was for drop spreading time, $t_S$.

The importance of contact angle hysteresis, $\Delta\theta$, is shown, e.g., by comparison of OTSb and Teflon, which have different $\theta_A$ (so, different spreading behavior, see Figure 5), but similar $\Delta\theta$ (so, similar $\Delta t_{\xi_{\max}}$, see Figure 6). The effect of $\Delta\theta$ on $\Delta t_{\xi_{\max}}$ is intuitive: as the contact angle hysteresis increases, more time is needed for the contact angle to change from the value reached during spreading to the value needed for the contact line to recede; as such, $\Delta t_{\xi_{\max}}$ increases with increasing $\Delta\theta$.

Also of interest is the observation that the effect of wettability is still present at highest $We$. This is a relevant issue, since in the literature it is generally recognized that at high $We$ numbers capillary effects are secondary; however, it is not always clear from which time wettability starts to play an important role. Figure 6 highlights that, even at high $We$, capillary effect plays an important role in shortening the time needed for recoil to start. This can be explained considering that as drop stops to spread and starts to recoil, contact line velocity (and, consequently, the capillary number, $Ca = \mu V_{cl}/\sigma$) is low and capillarity is not overcome by inertial effect even at high $We$, differently from the initial phase of spreading.

Results for time at maximum spreading, $\Delta t_{\xi_{\max}}$, highlights the role played by contact angle hysteresis, $\Delta\theta$, not only in static or quasi-static conditions (e.g., to predict drop mobility on a surface), but also during strongly dynamic events, such as drop impacts. These results further confirm the necessity to characterize surface wettability not only with a single value for the contact angle, but with a set of values. Contact angle hysteresis has a direct effect on drop impact characteristics, even for high energy impacts (up to $We = 685$ in the present study): high $\Delta\theta$ means that recoiling phase is retarded, whereas for low $\Delta\theta$ recoiling starts earlier.

## VI. CONCLUSIONS

Spreading of millimetric water drops impacting on dry surfaces has been investigated on hydrophilic to superhydrophobic surfaces, to evaluate the effect of surface wettability. Wetting properties are seen to have different influences, depending on drop impact conditions. For the investigated millimetric drop impacts, two spreading regimes were identified, based on the impact Weber number: for moderate Weber ($We < 200$), drop maximum spread factor, $\xi_{\max}$, and spreading time, $t_S$, are both influenced by wettability, characterized by the advancing contact angle, $\theta_A$, the surface parameter that best correlates to maximum spreading; for high Weber ($We > 200$), inertial effects become predominant over capillarity and the effect of wettability is negligible during spreading. With respect to maximum spread factor, $\xi_{\max}$, fitting of experimental data show that at high Weber numbers $\xi_{\max} \propto We^{0.20} \propto V^{0.40}$. At moderate Weber numbers ($We < 200$), maximum spread factor is related to Weber number and velocity as $\xi_{\max} \propto We^{0.26} \propto V^{0.52}$ (for glass, the most hydrophilic surface), and as $\xi_{\max} \propto We^{0.40} \propto V^{0.80}$ for superhydrophobic surfaces. Drop maximum spreading on the two SHSs was similar for all tested conditions, irrespective of eventual surface impalement (i.e., transition from Cassie to Wenzel wetting state). Comparing experimental data with correlations and models in the literature, we found that correlation by Roisman[11] is the one that best predicts drop spreading on a hydrophilic surface, whereas no correlations are able to predict the different trends for $\xi_{\max}$ at moderate and high $We$ (with the slope of the curve $\xi_{\max}(We)$ changing from 0.40 to 0.20 in a logarithmic plot).

It was also found that drop spreading scaling time changes with wettability. For the most hydrophilic surface tested (e.g., glass, with $\theta_A = 48^\circ$), drop spreading time scales as $t_S \propto We^{-0.25} \propto V^{-0.50}$ on the entire Weber range. As such, spreading time is not directly proportional to the convective time, $D_0/V$, which is often used to make time non-dimensional during drop impact analysis. For a SHS, it was found that drop spreading time is unaffected by impact velocity at moderate $We$; all other surfaces show intermediate trends, once again being $\theta_A$ the surface parameter the control parameter. At high $We$, $t_S \propto We^{-0.25} \propto V^{-0.50}$ for all surfaces.

## ACKNOWLEDGMENTS

The authors acknowledge Alenia Aermacchi for interest and financial support. The funding of Regione Lombardia through the grant "Strumenti innovativi per il progetto di sistemi antighiaccio per l'aeronautica" is acknowledged (C.A. and M.M.). A.A. acknowledges funding from NSERC and Canada Research Chair Program. The authors acknowledge D. Barona (University of Alberta), R. Rioboo, S. Goosens, and J. De Coninck (University of Mons) for surface preparation.

[1] A. Theodorakakos, T. Ous, M. Gavaises, J. M. Nouri, N. Nikolopoulos, and H. Yanagihara, "Dynamics of water droplets detached from porous surfaces of relevance to PEM fuel cells," J. Colloid Interface Sci. **300**, 673–687 (2006).
[2] C. Antonini, M. Innocenti, T. Horn, M. Marengo, and A. Amirfazli, "Understanding the effect of superhydrophobic coatings on energy reduction in anti-icing systems," Cold Regions Sci. Technol. **67**, 58–67 (2011).
[3] A. Yarin, "Drop impact dynamics: Splashing, spreading, receding, bouncing. . . ," Annu. Rev. Fluid Mech. **38**, 159–192 (2006).
[4] M. Marengo, C. Antonini, I. V. Roisman, and C. Tropea, "Drop collisions with simple and complex surfaces," Curr. Opin. Colloid Interface Sci. **16**, 292–302 (2011).
[5] B. Scheller and D. Bousfield, "Newtonian droplet with a solid surface," AIChE J. **41**, 1357–1367 (1995).
[6] S. Sikalo, M. Marengo, C. Tropea, and E. N. Ganic, "Analysis of impact of droplets on horizontal surfaces," Exp. Therm. Fluid Sci. **25**, 503–510 (2002).
[7] R. Rioboo, M. Marengo, and C. Tropea, "Time evolution of liquid drop impact onto solid, dry surfaces," Exp. Fluids **33**, 112–124 (2002).
[8] J. Fukai, Y. Shiiba, T. Yamamoto, O. Miyatake, D. Poulikakos, C. M. Megaridis, and Z. Zhao, "Wetting effects on the spreading of a liquid droplet colliding with a flat surface: Experiment and modeling," Phys. Fluids **7**, 236–247 (1995).
[9] M. Pasandideh-Fard, S. Chandra, and J. Mostaghimi, "A three-dimensional model of droplet impact and solidification," Int. J. Heat Mass Trans. **45**, 2229–2242 (2002).
[10] I. V. Roisman, E. Berberović, and C. Tropea, "Inertia dominated drop collisions. I. On the universal flow in the lamella," Phys. Fluids **21**, 052103 (2009).
[11] I. V. Roisman, "Inertia dominated drop collisions. II. An analytical solution of the Navier–Stokes equations for a spreading viscous film," Phys. Fluids **21**, 052104 (2009).
[12] D. Bartolo, C. Josserand, and D. Bonn, "Retraction dynamics of aqueous drops upon impact on non-wetting surfaces," J. Fluid Mech. **545**, 329–338 (2005).
[13] A. L. Biance, F. Chevy, C. Clanet, G. Lagubeau, and D. Quéré, "On the elasticity of an inertial liquid shock," J. Fluid Mech. **554**, 47–66 (2006).
[14] C. Clanet, C. Béguin, D. Richard, and D. Quéré, "Maximal deformation of an impacting drop," J. Fluid Mech. **517**, 199–208 (2004).
[15] T. Mao, D. Kuhn, and H. Tran, "Spread and rebound of liquid droplets upon impact on flat surfaces," AIChE J. **43**, 2169–2179 (1997).
[16] D. Richard, C. Clanet, and D. Quéré, "Surface phenomena: Contact time of a bouncing drop," Nature (London) **417**, 811 (2002).
[17] R. Rioboo, M. Voué, A. Vaillant, and J. De Coninck, "Drop impact on porous superhydrophobic polymer surfaces," Langmuir **24**, 14074–14077 (2008).
[18] G. Hartley and R. Brunskill, "Reflection of water drop from surfaces," in *Surface Phenomena in Chemistry and Biology*, edited by J. Danielli, K. Pankhurst, and A. Riddiford (Pergamon, 1958), pp. 214–223.
[19] S. Chandra and C. T. Avedisian, "On the collision of a droplet with a solid surface," Proc. R. Soc. London, Ser. A **432**, 13–41 (1991).
[20] L. H. J. Wachters and N. A. J. Westerling, "The heat transfer from a hot wall to impinging water drops in the spheroidal state," Chem. Eng. Sci. **21**, 1047–1056 (1966).
[21] Lord Rayleigh, "On the capillary phenomena of jets," Proc. R. Soc. London, Ser. A **29**, 71–97 (1879).
[22] X. Li, X. Ma, and Z. Lan, "Dynamic behavior of the water droplet impact on a textured hydrophobic/superhydrophobic surface: The effect of the remaining liquid film arising on the pillars' tops on the contact time," Langmuir **26**, 4831–4838 (2010).
[23] R. Bhola and S. Chandra, "Parameters controlling solidification of molten wax droplets falling on a solid surface," J. Mater. Sci. **34**, 4883–4894 (1999).
[24] M. Pasandideh-Fard, Y. Qiao, S. Chandra, and J. Mostaghimi, "Capillary effects during droplet impact on a solid surface," Phys. Fluids **8**, 650 (1996).
[25] H.-Y. Kim and J.-H. Chun, "The recoiling of liquid droplets upon collision with solid surfaces," Phys. Fluids **13**, 643–659 (2001).
[26] W. Li and A. Amirfazli, "A thermodynamic approach for determining the contact angle hysteresis for superhydrophobic surfaces," J. Colloid Interface Sci. **292**, 195–201 (2005).
[27] C. W. Extrand and Y. Kumagai, "Liquid drops on an inclined plane: The relation between contact angles, drop shape, and retentive force," J. Colloid Interface Sci. **170**, 515–521 (1995).
[28] E. Pierce, F. J. Carmona, and A. Amirfazli, "Understanding or sliding and contact angle results in tilted plate experiments," Colloid Surf. A **323**, 73–82 (2008).
[29] A. J. B. Milne and A. Amirfazli, "Drop shedding by shear flow for hydrophilic to superhydrophobic surfaces," Langmuir **25**, 14155–14164 (2009).

[30] R. G. Cox, "The dynamics of the spreading of liquids on a solid surface. Part 1. Viscous flow," J. Fluid Mech. **168**, 169–194 (1986).
[31] S. F. Kistler, "Hydrodynamics of wetting," in *Wettability*, edited by J. C. Berg (Marcel Dekker, New York, 1993), p. 311.
[32] I. V. Roisman, L. Opfer, C. Tropea, M. Raessi, J. Mostaghimi, and S. Chandra, "Drop impact onto a dry surface: Role of the dynamic contact angle," Colloids Surf., A **322**, 183–191 (2008).
[33] J. P. Rothstein, "Slip on superhydrophobic surfaces," Annu. Rev. Fluid Mech. **42**, 89–109 (2010).
[34] G. McHale, M. I. Newton, and E. J. Shirtcliffe, "Immersed superhydrophobic surfaces: Gas exchange, slip and drag reduction properties," Soft Matter **6**, 714–719 (2010).
[35] J. Delplanque and R. Rangel, "An improved model for droplet solidification on a flat surface," J. Mater. Sci. **32**, 1519–1530 (1997).
[36] P. Attané, F. Girard, and V. Morin, "An energy balance approach of the dynamics of drop impact on a solid surface," Phys. Fluids **19**, 012101 (2007).
[37] C. Stow and M. Hadfield, "An experimental investigation of fluid flow resulting from the impact of a water drop with an unyielding dry surface," Proc. R. Soc. London, Ser. A **373**, 419–441 (1981).
[38] H. Marmanis and S. T. Thoroddsen, "Scaling of the fingering pattern of an impacting drop," Phys. Fluids **8**, 1344–1346 (1996).
[39] R. Rioboo, M. Voué, H. Adão, J. Conti, A. Vaillant, D. Seveno, and J. De Coninck, "Drop impact on soft surfaces: Beyond the static contact angles," Langmuir **26**, 4873–4879 (2010).
[40] D. Barona and A. Amirfazli, "Producing a superhydrophobic paper and altering its repellency through ink-jet printing," Lab Chip **11**, 936–940 (2011).
[41] I. Bayer, A. Brown, A. Steele, and E. Loth, "Transforming anaerobic adhesives into highly durable and abrasion resistant superhydrophobic organoclay nanocomposite films: A new hybrid spray adhesive for tough superhydrophobicity," Appl. Phys. Express **2**, 125003–125003 (2009).
[42] M. Reyssat, A. Péin, F. Marty, Y. Chen, and D. Quéré, "Bouncing transitions on microtextured materials," Europhys. Lett. **74**, 306–312 (2006).
[43] D. Bartolo, F. Bouamrirene, and A. Buguin, "Bouncing or sticky droplets: Impalement transitions on superhydrophobic micropatterned surfaces," Europhys. Lett. **74**, 299–305 (2006).
[44] See supplementary material at http://dx.doi.org/10.1063/1.4757122 for Annex A—Transition from Cassie-Baxter to Wenzel state due to drop impact and Annex B—Comparison between experimental data and models for drop maximum spreading.
[45] R. Rioboo, C. Tropea, and M. Marengo, "Outcomes from a drop impact on solid surfaces," Atomization Sprays **11**, 155–165 (2001).